



**HAL**  
open science

# Deciphering fluid flow at the magmatic-hydrothermal transition: A case study from the world-class Panasqueira W–Sn–(Cu) ore deposit (Portugal)

Gaëtan Launay, Stanislas Sizaret, Laurent Guillou-Frottier, Eric Gloaguen, Filipe Pinto

## ► To cite this version:

Gaëtan Launay, Stanislas Sizaret, Laurent Guillou-Frottier, Eric Gloaguen, Filipe Pinto. Deciphering fluid flow at the magmatic-hydrothermal transition: A case study from the world-class Panasqueira W–Sn–(Cu) ore deposit (Portugal). *Earth and Planetary Science Letters*, 2018, 499, pp.1-12. 10.1016/j.epsl.2018.07.012 . hal-01955965

**HAL Id: hal-01955965**

**<https://brgm.hal.science/hal-01955965>**

Submitted on 14 Dec 2018

**HAL** is a multi-disciplinary open access archive for the deposit and dissemination of scientific research documents, whether they are published or not. The documents may come from teaching and research institutions in France or abroad, or from public or private research centers.

L'archive ouverte pluridisciplinaire **HAL**, est destinée au dépôt et à la diffusion de documents scientifiques de niveau recherche, publiés ou non, émanant des établissements d'enseignement et de recherche français ou étrangers, des laboratoires publics ou privés.



Distributed under a Creative Commons Attribution - NonCommercial - NoDerivatives 4.0 International License

1       **Deciphering fluid flow at the magmatic-hydrothermal**  
2       **transition: a case study from the world-class W-Sn-(Cu) ore**  
3       **deposit of Panasqueira (Portugal)**

4  
5       Gaëtan Launay<sup>1,2</sup>, Stanislas Sizaret<sup>1</sup>, Laurent Guillou-Frottier<sup>1,2</sup>, Eric Gloaguen<sup>1,2</sup> and Filipe  
6       Pinto<sup>3,4</sup>

7       (1)     ISTO, UMR7327, Université d'Orléans, CNRS, BRGM, F-45071 Orléans, France

8       (2)     BRGM, F-45060 Orléans, France

9       (3)     Beralt Tin & Wolfram, S.A., Geology Department, Barroca Grande, Portugal

10      (4)     Institute of Earth Sciences (ICT), Pole of University of Porto, Rua do Campo Alegre  
11           687, 4169-007 Porto, Portugal

12  
13  
14  
15  
16  
17  
18      Manuscript submitted to Earth & Planetary Science Letters, the 26<sup>th</sup> of January 2018  
19  
20  
21  
22  
23  
24  
25  
26  
27  
28  
29  
30  
31  
32  
33  
34  
35  
36  
37

38           **Abstract:** Deciphering the behavior of fluid flow at the magmatic-hydrothermal transition is  
39 crucial to understand physical processes leading to the formation of intrusion-related ore deposits  
40 and hence to predict the localization of mineralized bodies. However, the hydrodynamics  
41 (direction and velocity) of the hydrothermal fluid flow related to this transitional stage remains  
42 poorly constrained. Here we present a coupled textural and chemical study performed on  
43 tourmaline growth bands to constrain fluid flow during the initiation of the hydrothermal system  
44 of the W-Sn-(Cu) Panasqueira deposit. This exceptional deposit consists of a dense network of flat  
45 wolframite and cassiterite-bearing quartz veins intensely developed above a well-known hidden  
46 greisen cupola. The W-Sn mineralization is preceded by a tourmalinization stage occurring as  
47 metasomatic halos around veins and as selvages developed along the vein-wall-rocks contacts.  
48 Results emphasize the key role of the greisen cupola on fluid focusing and the role of fluid  
49 overpressure during the vein opening. Velocity values highlight an efficient transport of metals in  
50 veins largely dominated by advective process ( $10^{-4}$  to  $10^{-3}$  m.s<sup>-1</sup>), whereas fluid flow in the altered  
51 wall-rocks is slow and pervasive ( $10^{-6}$  to  $10^{-5}$  m.s<sup>-1</sup>), suggesting that the element transport through  
52 the metasedimentary host rock was low and limited to the alteration haloes. LA-ICP-MS analyses  
53 of tourmaline growth bands reveal that fluids coming from the cupola are enriched in Na, K, Li, Sr  
54 and Sn, thus emphasizing the contribution of magmatic fluids during the vein formation and the  
55 metasomatic alteration of the wall-rocks. More generally, this study demonstrates that the apical  
56 portions of granite bodies play as emanative centers of mineralized fluids, and highlights the  
57 usefulness of mineral growth band analysis in the search for intrusion-related mineralization.

58  
59           **Keywords:** magmatic-hydrothermal activity, Panasqueira, tourmaline, growth bands, flow  
60 direction, flow velocity

## 66 **1. Introduction**

67 The formation of hydrothermal ore deposits and the development of alteration halos in rocks  
68 involve the transfer of a large amount of fluids through permeable rocks during several episodic  
69 pulses integrated over a long period of time (Barnes, 1997; Robb, 2005). To form a high-grade  
70 deposit, the flow of metal bearing fluids must be focused in a restricted space and coupled with an  
71 efficient precipitation and trapping mechanism. Hence, understanding hydrothermal fluxes  
72 constitutes a major issue of metallogeny and requires resolving some fundamental questions  
73 related to: (i) the driving force of fluid flow and (ii) the direction and the velocity of fluid flow.  
74 The search for answers to these issues involves a combination of approaches including recognition  
75 of permeable pathways (Sibson, 1992; Cox 2005), mineralogical and geochemical analysis  
76 (Cartwright and Buick, 1996; Ferry et al., 2002) and fluid hydrodynamics (Ingebristen and  
77 Appold, 2012).

78 Among hydrothermal ore deposits, those triggered and driven by magmatic felsic intrusions  
79 represent a main primary source of economically important metals, including copper (Cu),  
80 tungsten (W), tin (Sn), molybdenum (Mo) and gold (Au) (Hedenquist and Lowenstern, 1994;  
81 Černý et al., 2005). There is general agreement that these magmatic-related deposits are partly  
82 formed by releasing and expulsion of metal-bearing fluids during the emplacement and the cooling  
83 of magmatic intrusions (Hedenquist and Lowenstern, 1994; Černý et al., 2005). Another important  
84 process for metal transport in magmatic-hydrothermal systems is the development of large  
85 convective cells around plutons driven by the thermal contrast between intrusive bodies and the  
86 host rocks. This convective fluid flow is able to mobilize a large amount of fluids from the  
87 surrounding host rock and has a marked effect on the fluid flow patterns (Norton and Cathles,  
88 1979; Eldursi et al., 2009). More specifically, it has been commonly observed that mineralized  
89 systems are usually centred on small plutons, apices or feeder zones (Dines, 1956; Dilles and  
90 Proffett, 1995; Gloaguen et al., 2014) suggesting a strong control of the pluton roof geometry on  
91 mineralizing fluid flow. Indeed, some numerical models have demonstrated that fluid flow is  
92 optimal above the apical part of intrusions and predict the formation of ore deposits in these areas

93 (Sams and Thomas-Betts, 1988; Eldursi et al. 2009; Weis et al. 2015). Despite these elegant  
94 numerical results, this expected fluid flow pattern (flow direction and velocity) needs to be  
95 verified by field investigations.

96 Moreover, it is widely recognized that magmatic-hydrothermal systems integrate a complex  
97 history encompassing episodic stages of fluid flow related to polyphase intrusion emplacement,  
98 which have important effects on the geometry of hydrothermal systems. In this scheme, the  
99 magmatic-hydrothermal transition is a key event that marks the initiation of the hydrothermal  
100 system and defines the future behavior of fluid flow. Indeed, it is usually during this transitional  
101 stage that permeable structures open and drain mineralized fluids. However, fluid flow related to  
102 this specific hydrothermal stage is difficult to access and thus remains poorly constrained due to  
103 the lack of recognized methods to implement in the field.

104 The textural analysis of mineral growth bands has provided significant information about the  
105 direction and velocity of fluid flow involved in the formation of hydrothermal ore deposits  
106 (Kessler et al. 1972) and during metasomatic processes (Sizaret et al., 2009; Majhoubi et al.,  
107 2016). This direct approach constitutes a powerful tool to constrain fluid flow related to a specific  
108 hydrothermal event such as the magmatic-hydrothermal transition. In the present study, we  
109 perform a textural analysis of tourmaline growth bands to decipher fluid flow at the initiation of  
110 the magmatic-hydrothermal stage of Panasqueira (Portugal). This textural analysis is combined  
111 with trace elements analysis of tourmaline growth bands to constrain the chemical characteristics  
112 of fluids from which the tourmalines have crystallized. Panasqueira is an historic world-class W  
113 vein deposit characterized by a well-preserved magmatic-hydrothermal plumbing system. This  
114 deposit is one of the best-documented and characterized in the world and represents a reference  
115 site to study magmatic-hydrothermal processes leading to the formation of a Sn-W ore deposit  
116 (Thadeu, 1951; Kelly and Rye 1979; Poyla, 1989; Poyla et al., 2000; Foxford et al., 2000;  
117 Lecumberri-Sanchez et al., 2017; Codeço et al., 2017). From the results of estimated fluid  
118 directions and velocities, we discuss the key parameters controlling the behavior of fluid flow at  
119 different scales, such as: (i) the role of granitic cupolas on the localization of mineralized areas by  
120 fluid flow focusing, (ii) the role of fluid overpressure conditions on vein opening and propagation

121 of alteration halos in wall-rocks, and (iii) the required duration of fluid flow during the W-Sn  
122 mineralization stage.

## 123 **2. Geological and metallogenic framework**

### 124 *2.1 Regional geology*

125 The W-Sn-(Cu) Panasqueira ore deposit is located in the Central Iberian Zone (CIZ), which  
126 constitutes the axial zone of the Iberian Variscan belt (Fig. 1a) (Julivert et al., 1972). The CIZ is  
127 composed of the Schist-Greywacke-Complex (SGC) intruded by a large volume of granitoid  
128 intrusions resulting from an extensive magmatic event during the latest stages of the Variscan  
129 orogeny (Dias et al., 1998). The SGC consists of a thick (8-11 km) sequence of late  
130 Neoproterozoic schists and greywackes affected by a regional greenschist metamorphism  
131 (Martínez-Catalán et al., 2007). Deformation of the SGC consists of tight and upright folds with  
132 NW-SE sub-vertical axial planes produced by a NE-SW shortening related to the earliest  
133 compressive stage of the Variscan orogeny (Dias and Ribeiro, 1995 and Martínez-Catalán et al.,  
134 2007). This folding is associated with a regional sub-vertical penetrative axial planar cleavage (S1)  
135 (Fig. 1a and 1b). The CIZ host numerous Sn-W ore deposits and occurrences related to granitic  
136 intrusions and formed by magmatic-hydrothermal processes (Derré, 1982).

137

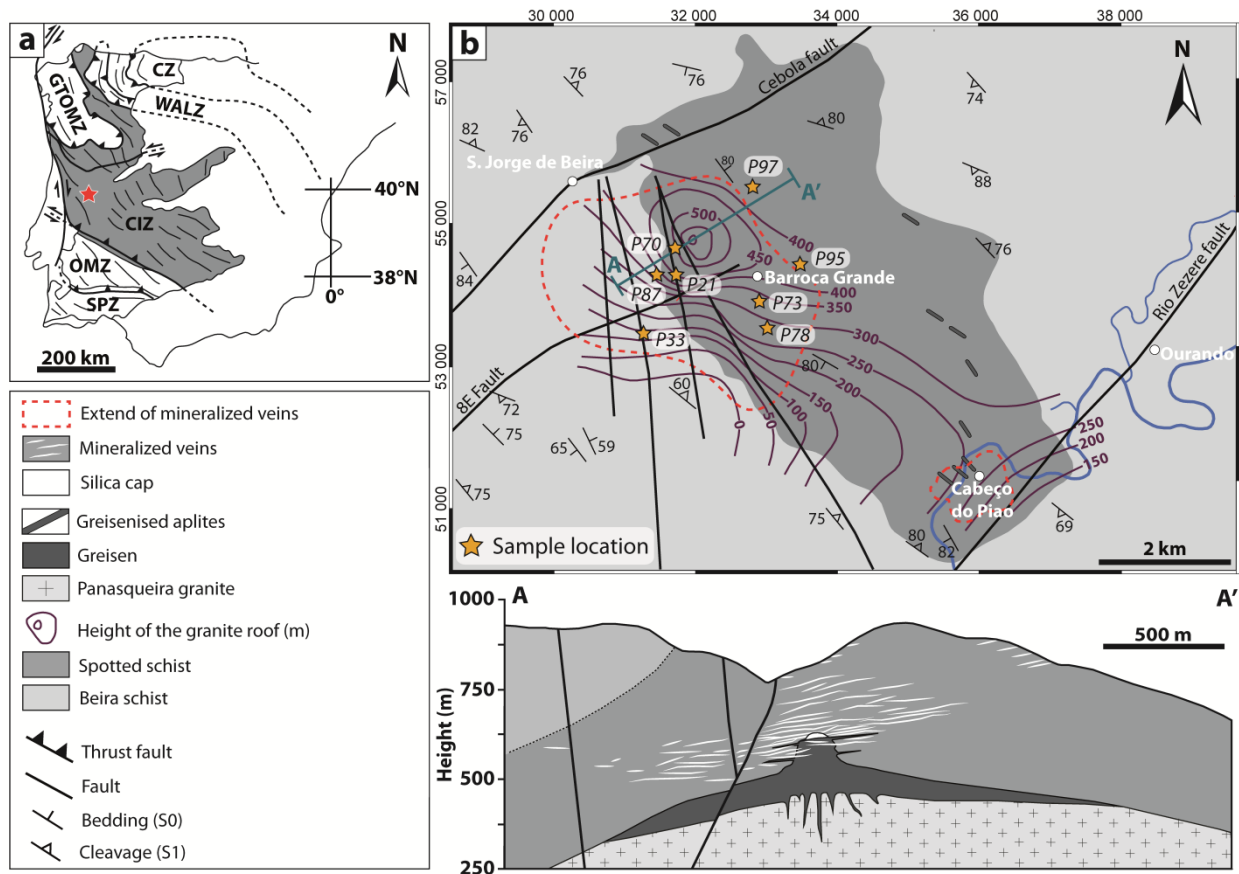


**Figure 1 (a) Tectonic map of the Variscan Iberian massif showing the main tectonostratigraphic domains defined by Julivert *et al.*, (1972). The location of the Panasqueira deposit is marked by a red star. CZ: Cantabrian Zone, WALZ: West Asturian-Leonese Zone, GTOMZ: Galicia Tràs-os-Montes Zone, CIZ: Central Iberian Zone, OMZ: Ossa-Morena Zone and SPZ: South Portuguese Zone (b) Geological map of the Panasqueira ore deposit including the height of the granite roof. The (A-A') geological cross section displaying the spatial relationship between mineralized veins and the greisen cupola (data source Beralt Tin & Wolfram S.A.).**

138

## 139 2.2 The W-Sn-(Cu) Panasqueira ore deposit

140 The Panasqueira ore deposit is located in the Beira Baixa province in the southern flank of the  
 141 Serra da Estrela massif constituted by late to post tectonic granitic intrusions. In this region the  
 142 late Neoproterozoic folded and metamorphosed SGC is locally named Beira Schist. At  
 143 Panasqueira, spotted schists mark the presence of a thermal metamorphic aureole related to an  
 144 underlying S-type granite (Thadeu, 1951; Clark, 1964). The intrusive body is limited by the  
 145 Cebola fault to the north and the Rio Zêzere fault to the south (Fig. 1b) (Clark, 1964). As exposed  
 146 by underground mining works and drill cores, the upper part of this granite includes a quartz-

147 muscovite greisen cupola formed by interaction between granitic rocks and acidic F-B and Li-rich  
148 fluids (Shcherba, 1970; Bishop, 1989) (Fig. 1b and 2a).

149 The W-Sn mineralization is hosted by a dense network of low dipping veins crosscutting the  
150 vertical foliation of the Beira Schist and the greisen cupola (Fig. 2a). The veins system is centered  
151 above the greisen cupola and extends over an area of 6 km<sup>2</sup> for a depth extension of about 200-300  
152 meters (Fig. 1b) (Kelly and Rye 1979; Poyla et al., 2000). This unusual shallow dipping  
153 orientation of mineralized veins is compatible with the regional stress field that involved NE-SW  
154 shortening with a vertical  $\sigma_3$  leading to the formation of tight and upright folds accompanied by  
155 the development of the regional NW-SE sub-vertical foliation (Dias and Ribeiro, 1995; Martínez-  
156 Catalán et al., 2007). Based on textural and structural analysis of the vein swarms, Foxford et al.,  
157 (2000) proposed a crack-and-seal model involving episodic vein dilation and filling induced by  
158 injections of fluids at supralithostatic pressure conditions in a compressive crustal regime.  
159 Although this mechanism is quite appealing, these conditions of fluid overpressure in veins remain  
160 unproven. The structural control of the vein formation has probably induced permeability  
161 anisotropy with a strong horizontal component which could affect the pattern of fluid flow at the  
162 mineralization time. A late NNW-SSE and ENE-WSW sub-vertical fault system crosscuts the  
163 veins and the granite intrusion (Fig. 1b) (Thadeu 1951, Kelly and Rye 1979, Foxford et al., 2000).  
164 As evidence in the field, these faults postdate mineralization event and have not controlled fluid  
165 flow during the W-(Sn) mineralization (Thadeu, 1951).

166 The complex paragenetic sequence of veins was described in detail by Kelly and Rye (1979)  
167 and improved by Poyla et al., (2000). At least five mineralization stages occurred in the veins  
168 from oldest to youngest: the Quartz-Tourmaline (QTS) stage, the Main Oxide Silicate Stage  
169 (MOSS), the Main Sulfide Stage (MSS), the Pyrrhotite Alteration Stage (PAS) and the Late  
170 Carbonate Stage (LCS). The MOSS (Fig. 2b) and the MSS (Fig. 2c) are the most economically  
171 relevant ore stages. The MOSS carries the W-Sn mineralization and consists in muscovite and  
172 quartz accompanied by wolframite and cassiterite. The two earliest mineralization stages (QTS  
173 and the MOSS) constitute a continuous sequence which is then superimposed and/or cross-cut by  
174 the late sulfide stage (MSS). The MSS, which carries the Cu mineralization, is mainly composed

175 of arsenopyrite, chalcopyrite, sphalerite pyrite and pyrrhotite (Thadeu 1951, Kelly and Rye 1979,  
176 Poyla *et al.* 2000). Based on fluid inclusions analyses, Kelly and Rye (1979) and Bussink (1984)  
177 have reported that fluids related to the MOSS and the QTS have been trapped at temperatures  
178 between 300 and 350°C. Although the tourmaline stage (QTS) is volumetrically of minor  
179 importance (mm to cm of thickness), it marks the initiation of the Panasqueira hydrothermal  
180 system (Poyla *et al.*, 2000).

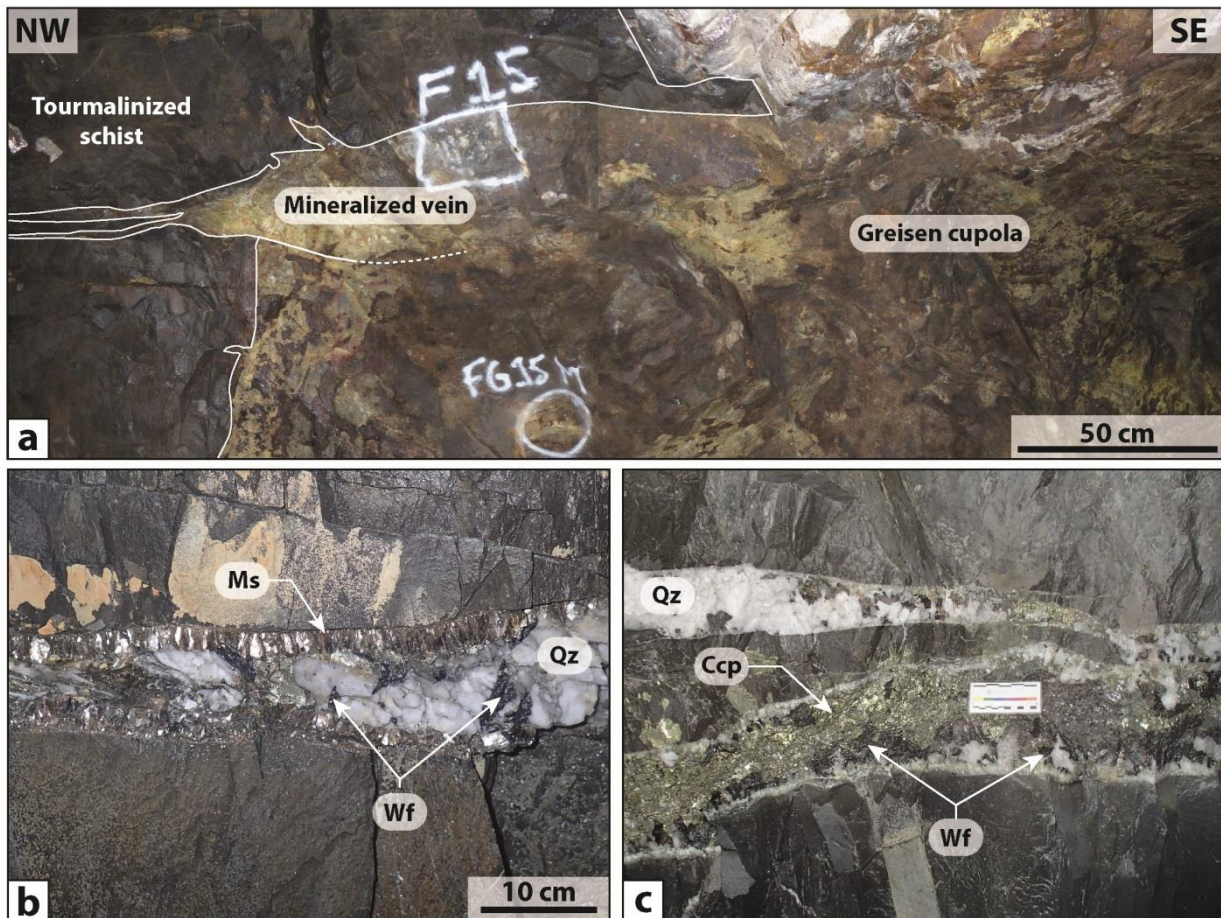


Figure 2 The mineralized system of the W-Sn-(Cu) Panasqueira deposit. (a) Contact between the greisen cupola and the tourmalinized metasedimentary host rock at the level 1 of the mine. Note the presence of mineralized veins which crosscut this contact. (b) Typical Quartz-Wolframite veins corresponding to the main oxide stage. (c) Quartz-Wolframite veins superimposed by the late sulfide stage carrying the Cu mineralization. Abbreviation from Whitney and Evans (2010) Ccp: Chalcopyrite, Ms: Muscovite, Qz: Quartz and Wf: Wolframite.

181  
182  
183  
184

185 **3. Tourmaline occurrence**

186 At Panasqueira, tourmaline is common, especially in metasedimentary host rock surrounding  
187 mineralized veins (Fig. 3a). Tourmaline is present within alteration halos, which are developed  
188 along schist-vein contacts within the lower and the upper wall-rocks. These halos result from  
189 metasomatic reactions induced by fluid–rock interactions during hydrothermal fluid flow in the  
190 veins. Locally, it is possible to observe alternation of quartz-rich and tourmaline-muscovite rich  
191 layers inherited from lithological heterogeneities of the Beira Schist. These tourmalines are fine  
192 and their trigonal axes are randomly oriented in the vertical cleavage planes of the schist.

193 Tourmaline is also present in veins along schist-vein contacts  
194 (Fig. 3b and 3c). They occur as fine acicular crystals (1-3 mm) with  $\langle c \rangle$  axes vertical and  
195 perpendicular to the vein edge and consequently to the inferred plane of fluid flow (Fig. 3c). These  
196 tourmalines grains are commonly associated with apatite, rutile and muscovite (Fig. 3d), while  
197 their relation with the ore minerals (wolframite and cassiterite) is difficult to observe. However, in  
198 some veins tourmaline appears to shortly predate wolframite and can be texturally associated with  
199 cassiterite (Fig. 3e). Consequently, tourmaline represents a good candidate to track W-Sn  
200 mineralized fluid flow related to the QTS and the MOSS in the Panasqueira veins system.

201 For both types of tourmaline, the sections normal to the  $\langle c \rangle$  axis are characterized by growth  
202 band zonation with a core and well-defined rims (Fig. 3d and Fig. 3f). These bands emphasize an  
203 anisotropic growth and highlight a symmetry breakdown due to a directional fluid flow (Fig. 4a  
204 and 4b).

205

206

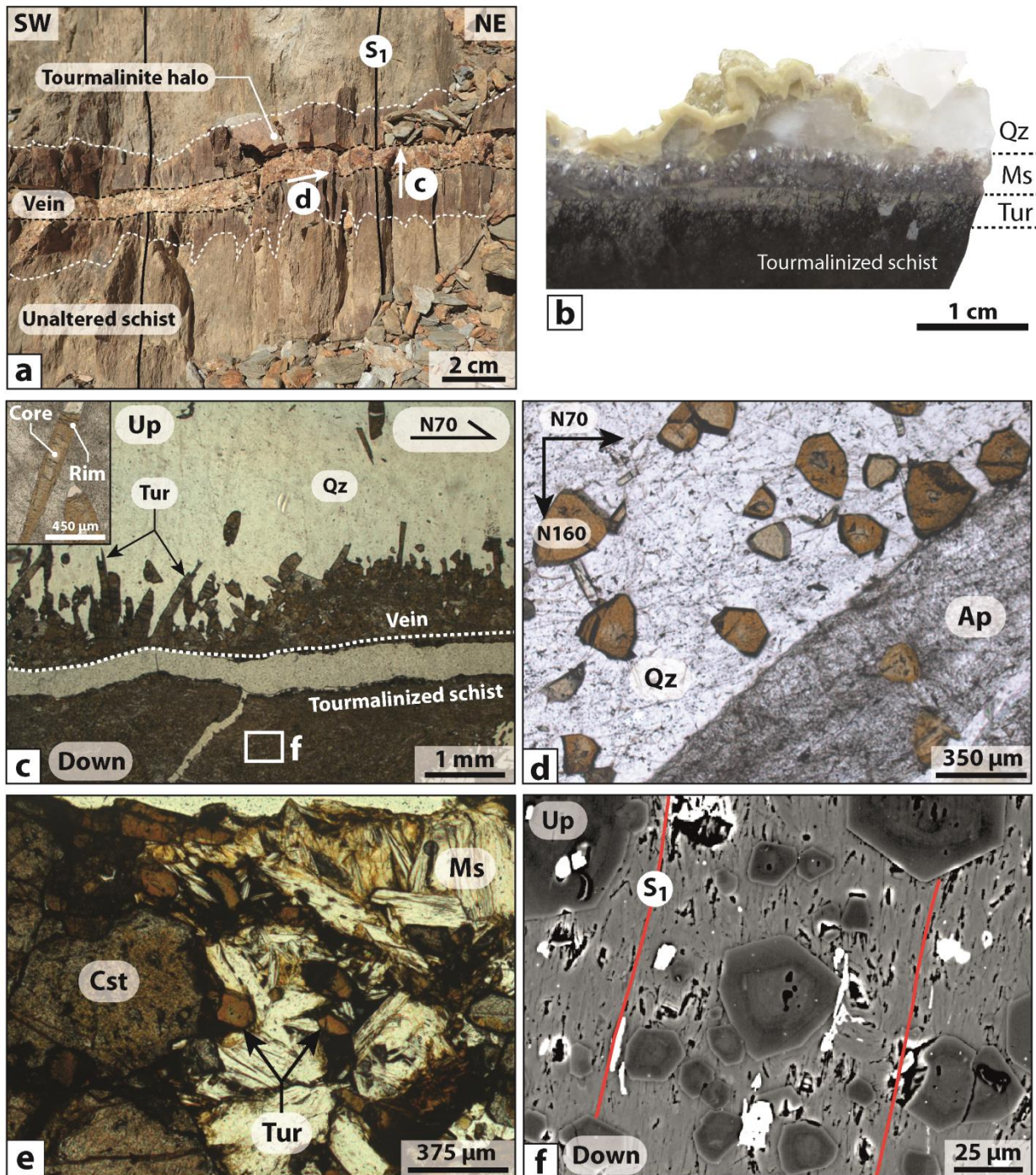


Figure 3 Textural and petrographic characteristics of tourmalines present in the mineralized system of Panasqueira. (a) Quartz-tourmaline vein with tourmalinization of the metasedimentary wall-rocks. The white dashed line indicates the tourmalinization front in the metasedimentary host rock. c and d arrows give orientation of the thin sections c and d. Note the preferential migration of tourmalinization front in the vertical foliation planes  $S_1$  (b) Sample of mineralized veins showing the vertical growth of acicular tourmalines along the schist-vein contact. (c) and (d) photomicrographs of vein tourmaline showing sections parallel (c) and normal (d) to the trigonal axis of tourmaline. (e) Photomicrograph of mineralized vein showing tourmaline grains associated with cassiterite. (f) SEM photomicrograph of altered schist perpendicular to the foliations planes showing growth band zoning in tourmaline basal sections. Abbreviation from Whitney and Evans (2010) Ap: Apatite, Cst: Cassiterite, Ms: Muscovite and Qz: Quartz.

## 4. Sampling and methodology

Owing to its remarkable mechanical and chemical stability, tourmaline is able to record significant information about its host environment (Henry and Dutrow, 1996; Van Hinsberg et al. 2011a). In particular, tourmaline provides a powerful tool to constrain hydrodynamics (direction and velocity of fluid flow) of geological processes involving fluid flow (Sizaret et al., 2009; Mahjoubi et al., 2015). Moreover, tourmaline incorporates a diversity of trace elements and constitutes a geochemical monitor of fluid compositions (Marks et al., 2013; Van Hinsberg et al., 2017). In this study, tourmaline growth bands were used to track both flow and chemical composition of hydrothermal fluids involved during the earliest stages of the vein formation at Panasqueira.

Oriented vein samples with tourmaline were collected in the mine and at the surface, at different places around the cupola, both horizontally and vertically to have a full spatial distribution, and to establish a paleo-fluid flow map around the granitic intrusion (Fig. 1b). Unfortunately, no samples were available in the northwestern part of the studied area.

The vertical migration of the alteration front (tourmalinization) within the metasedimentary host rocks appears to be driven by the sub-vertical foliation planes (S1). To study the vertical fluid flow related to the alteration of the wall-rocks, samples of alteration halos have been collected above and below veins perpendicularly to the vertical foliation planes (NE-SW section). The orthogonal NW-SE sections are parallel to the foliation planes and hence do not permit to perform fluid flow reconstruction in the wall rock due to the preferential crystallization of tourmaline in parallel within the foliation planes.

### 4.1 Fluid flow reconstruction by growth band measurements

In hydrothermal systems, the crystal shape is controlled by its intrinsic symmetry and the effects of external forces, such as fluid flow, that induce anisotropic growth (Curie 1908). The method used for reconstruction of local fluxes is based on the notion that crystal faces exposed to the chemical flux (i.e. the upstream faces) grow faster than downstream faces (Kessler et al. 1972 and Sizaret et al., 2006 and 2009). The relationship between flow velocity and the relative growth

234 rate of upstream and downstream faces can be modelled and quantified (Sizaret et al. 2006 and  
235 2009). From this postulate, it is possible to deduce local fluid flow directions and velocities in the  
236 hydrothermal system. Oriented thin sections were cut parallel to the expected stream-line, i.e.  
237 parallel to veins, within the vein, and vertically and perpendicular to foliation planes in altered  
238 host rocks. Tourmaline crystals were examined on polished thin sections using optical transmitted  
239 light and scanning electron microscope. Then, on tourmaline basal section (i.e., perpendicular to  
240 the trigonal axis) the growth band thickness of equivalent crystal faces ( $d_1$ ,  $d_2$  and  $d_3$ ) and their  
241 respective directions ( $\alpha_1$ ,  $\alpha_2$  and  $\alpha_3$ ) have been measured (Fig. 4c). The three normalized  
242 thicknesses  $d_{\max}$ ,  $d_{\text{int}}$  (intermediate) and  $d_{\min}$  were determined. Assuming that the thickest band  
243 ( $d_{\max}$ ) received the largest chemical flux, the orientation of  $d_{\max}$  gives the direction of the paleo-  
244 fluid flow recorded by the crystal (Fig. 4c).

245 The relationship between fluid velocity and growth ratios ( $d_{\max}/d_{\min}$ ) was established by  
246 solving the coupled Navier-Stokes and chemical transport equations with the Comsol Multiphysics  
247 finite element code (Sizaret et al., 2009). In this modeling the edge size of tourmaline is 50  $\mu\text{m}$   
248 and the fluid (water) viscosity is chosen at realistic mineralizing conditions, taken here at 350°C  
249 ( $7.3 \cdot 10^{-5}$  Pa.s source NIST WebBook, 2017). Varying flow velocity provides a relationship  
250 between chemical flux ratio (upstream/downstream) and fluid velocity (Fig. 4d). The growth band  
251 thicknesses measured on minerals can be considered as chemical fluxes integrated over a given  
252 period of time. Consequently, the fluid velocity can be determined by inverse method by reporting  
253 the measured  $d_{\max}/d_{\min}$  ratio on the flux ratio (Upstream/downstream) vs velocity curve (Fig. 4d)  
254 (Sizaret et al. 2006 and 2009).

255 To obtain representative measurements, basal sections of tourmaline were chosen from the  
256 following criteria: absence of contact with another crystal of tourmaline, absence of  
257 recrystallization and corrosion and easily identifiable equivalent faces.  
258 For each site, flow directions and velocities deduced from each tourmaline section were  
259 implemented and treated with the free meteorological software WRPLOT View™ (Lake  
260 Environmental, 2016) in order to establish “wind roses” of local paleo-fluid flow. These rose  
261 diagrams are then reported on the map.

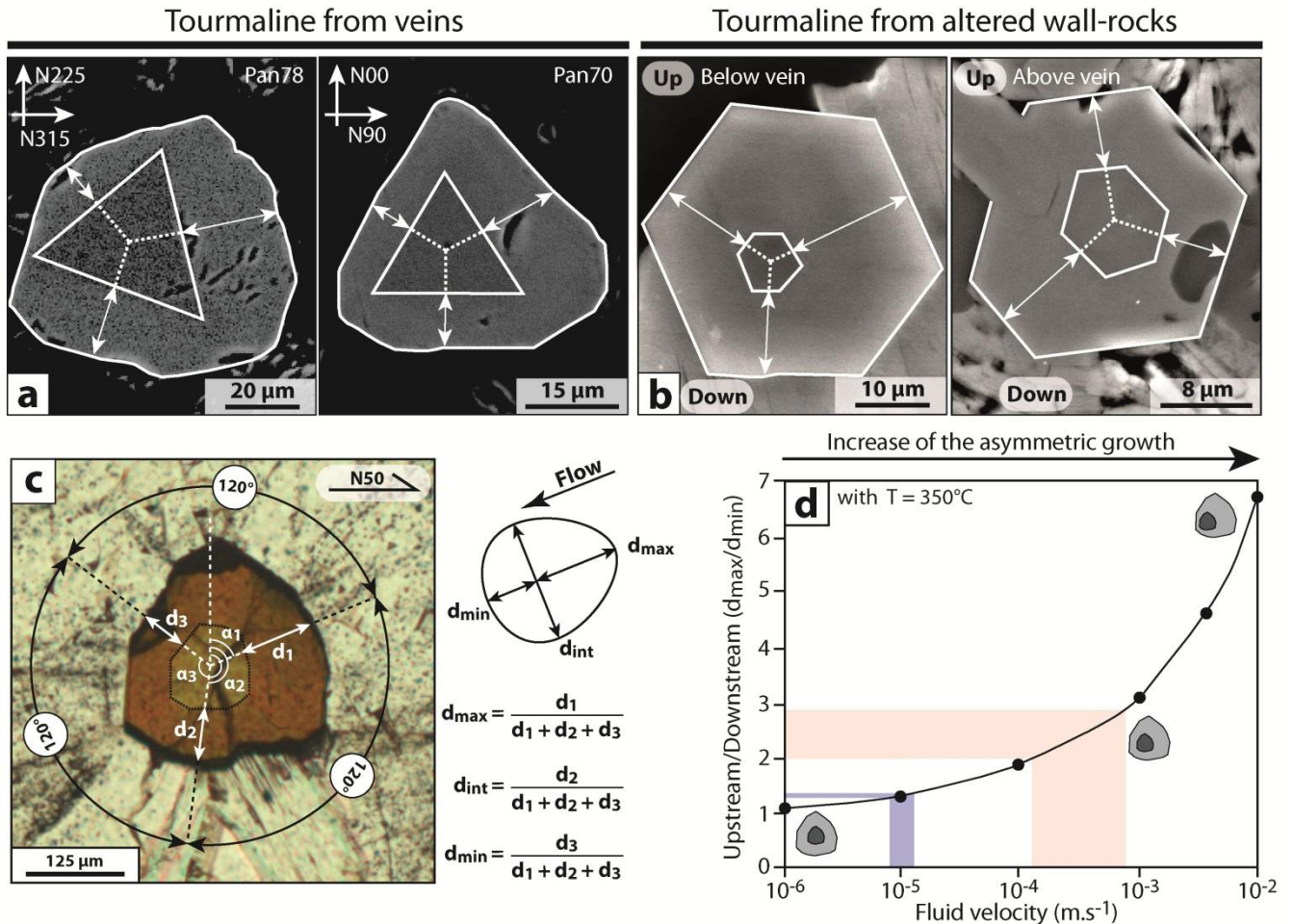


Figure 4 Examples of basal sections of tourmaline from veins (a) and altered wall-rocks (b) displaying an asymmetric shape due to an anisotropic growth (c) Measurements of growth bands thickness and orientation on a basal section of tourmaline. (d) Curve deduced from numerical modeling showing relationship between fluid velocity and flux ratio (see text for details). The filled boxes indicate range of averages of fluid velocities derived from  $d_{max}/d_{min}$  ratio measured on tourmalines from altered wall-rocks (blue) and veins (red).

262

## 263 4.2 Tourmaline growth band chemistry

### 264 4.2.1 Major and minor element analysis

265 The major and minor element compositions of tourmaline were determined on polished thin  
 266 sections using a Cameca SX-Five electron probe micro-analyzers (EPMA) at the Institut des  
 267 Sciences de la Terre d'Orléans (ISTO). Analyses were performed using an accelerating voltage of  
 268 15 kV, a beam current of 6 nA with a diameter of 2 μm. The elements analyzed were Si, Ti, Al,  
 269 Fe, Mn, Mg, Ca, Na, K, F and Cl. For calculation of the structural formulae and site allocation in  
 270 tourmaline, analyses were normalized to 15 cations (T + Z + Y-sites) and B<sub>2</sub>O<sub>3</sub> and H<sub>2</sub>O contents

271 were calculated by stoichiometry, considering B = 3 apfu and OH + F + Cl = 4 apfu. Analytical  
272 conditions and calibration are detailed in electronic supplementary materials (ESM1).

#### 273 4.2.2 Trace element analysis

274 Trace element concentrations in tourmaline were determined by laser ablation inductively  
275 coupled plasma-mass-spectrometry (LA-ICP-MS). These analyses were performed at BRGM  
276 (French Geological Survey) using a ThermoScientific X series II quadrupole ICP-MS coupled  
277 with a Cetac Excite 193 nm laser ablation system. Ablations were performed with a repetition rate  
278 of 8Hz and laser energy of 3.5 J/cm<sup>2</sup> with a beam size of 40 µm. Analyses comprise 20 seconds of  
279 gas blank measurement following by 60 seconds of ablation. Elements analyzed were <sup>7</sup>Li, <sup>23</sup>Na,  
280 <sup>24</sup>Mg, <sup>27</sup>Al, <sup>29</sup>Si, <sup>47</sup>Ti, <sup>51</sup>V, <sup>55</sup>Mn, <sup>66</sup>Zn, <sup>88</sup>Sr and <sup>118</sup>Sn. Data reduction was performed with the  
281 software Glitter 4.0 using the NIST SRM-612 glass standard for external standardization and <sup>29</sup>Si  
282 as the internal standard. Concentrations in Mg and Al obtained by LA-ICP-MS data reduction  
283 were compared with EPMA analyses to check the accuracy of the results. Analyses of certified  
284 standard NIST-612 SRM give a good accuracy with a relative standard deviation (RSD) below  
285 10%. Detection limits for most elements range between 0.2 and 5 ppm. Higher detection limits  
286 were achieved for Zn, Ti and Na (respectively 5.5 ppm, 15.4 ppm and 37.4 ppm).

## 287 5. Results

### 288 5.1 Large scale fluid flow

289 Fluid flow directions and velocities are summarized in Table 1 (complete measurements in  
290 electronic supplementary materials ESM2) and illustrated in Figure 5. For veins-hosted  
291 tourmaline, an average ratio of  $d_{\max}/d_{\min}$  was determined for each of the 8 sample sites. These  
292 average ratios range from 2.0 to 2.9 implying a fluid velocity varying from 10<sup>-4</sup> to 10<sup>-3</sup> m.s<sup>-1</sup> in  
293 veins (Table 1 and Fig. 4d). Figure 5c shows the histogram representation of all velocity values,  
294 which are characterized by an asymmetric distribution centered on 10<sup>-4</sup> - 5.10<sup>-4</sup> m.s<sup>-1</sup>. This wide  
295 variable distribution is probably due to the sinuous nature of the fluid flow path. Indeed, a  
296 narrowing of the pathway can be responsible of the local high velocity value recorded by some  
297 tourmalines. For each sample of veins, the flow directions are dispersed with a significant mean

298 direction (Fig. 5a). In the “rose” diagrams, these directions generally host the highest velocity  
299 values ( $10^{-4}$  to  $10^{-3}$  m.s<sup>-1</sup>). Conversely, lowest fluid velocity values are not aligned with these mean  
300 directions of fluid flow (Fig. 5a). Considering all the sites, the mean orientations of flow depict a  
301 large-scale streamline structure with radial directions coming from a center located on the greisen  
302 cupola (Fig. 5a and 5b). The vertical fault system crosscutting the veins does not influence flow  
303 direction in the veins (Fig. 5b). The pitch of flow direction vectors on the vein plane is not aligned  
304 to the dip direction of veins (Table 1). Consequently, flow directions are not influenced by veins  
305 orientation.

### 306 *5.2 Fluid flow in host rock*

307 In altered schist, tourmaline growth bands show a fluid flow escaping sub-vertically from  
308 veins toward the host rock, with an averaged angle of 55° above and 60° below the vein (Fig. 6).  
309 This symmetrical behavior may be related to the horizontal component of fluid flow within the  
310 vein, as suggested by measurements on the P21 sample. Mean velocities obtained in altered wall-  
311 rocks are 1 to 2 orders of magnitude lower than fluid velocity obtained in the veins (Fig. 4d and  
312 Fig. 6). In addition, it would appear that velocities are higher above ( $10^{-5}$ -  $5.10^{-5}$  m.s<sup>-1</sup>) than below  
313 veins ( $5.10^{-6}$  to  $10^{-5}$  m.s<sup>-1</sup>) (Fig. 6).

314

315

316

317

318

319

320

321

322

323

324

325

326

Veins:	Coordinates (ETR S89/Portugal TM06)			Veins orientation		$d_{\max}/d_{\min}$			Fluid flow		
	X (m)	Y (m)	Z (m)	Strike	Dip	N	Mean	SD	Mean direction	Mean velocity (m.s <sup>-1</sup> )	Pitch
Pan70	31675.9	54649.3	620	N136	7°	30	2.06	0.66	N28	2.76E-04	77°
Pan87	31410.9	54261.6	620	N300	5°	41	2.50	0.95	N64	6.65E-04	60°
Pan21	31675.1	54253	560	N200	5°	31	2.06	1.06	N27	5.53E-04	10°
Pan33	31217.9	53385.2	470	N130	15°	24	2.24	0.39	N40	3.33E-04	90°
Pan78	33043.4	53490.3	618	N138	7°	31	2.29	1.13	N331	6.66E-04	26°
Pan73	32933.2	53875.3	662	N127	10°	25	2.75	1.10	N321	9.46E-04	24°
Pan95	33058.4	54287	741	N127	5°	18	2.92	1.27	N300	1.38E-03	8°
Pan97	32833.3	55559.5	732	N160	10°	25	2.74	0.96	N201	9.47E-04	42°
<b>Altered wall-rocks :</b>											
P20 Up	31675.1	54253	560	-	-	28	1.36	0.18	55	1.44E-05	-
P20 Down	31675.1	54253	560	-	-	28	1.29	0.11	60	6.95E-06	-

327 **Table 1 Results of directions and velocities of fluid flow deduced from tourmalines growth bands in veins and in altered wall-rocks (SD: Standard Deviation and N:**  
328 **number of measurement).**

329

330

331

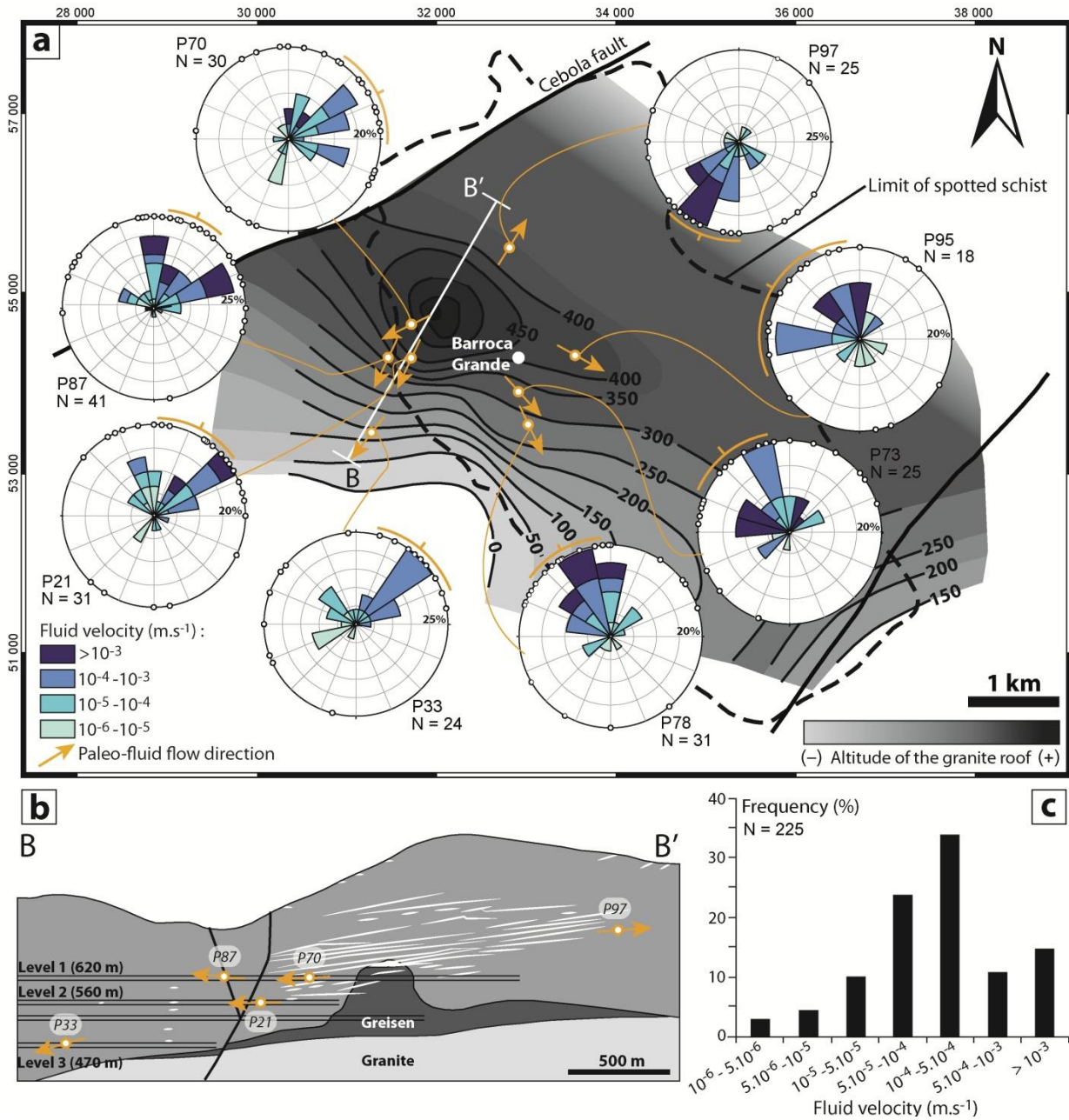


**Figure 5** Results of fluid flow at the ore deposit scale deduced from tourmaline growth bands in mineralized veins. (a) Large scale map of paleo-fluid flow around the hidden granite of Panasqueira. Local fluid flow direction and velocities are represented with “rose” diagrams, which give direction of tourmaline faces exposed to the fluid flow ( $d_{max}$ ) and directional distribution of fluid velocities. The orange arcs give the 95% interval of confidence, from where the fluid comes. The orange arrows on the map correspond to the mean directions of flow determined for each sample site. N corresponds to the number of measurements performed for each sample sites. (b) Results of fluid flow projected on the geological cross section (B-B') showing flow moving away from the cupola. (c) Histogram showing distribution of all fluid velocity values.

332

333

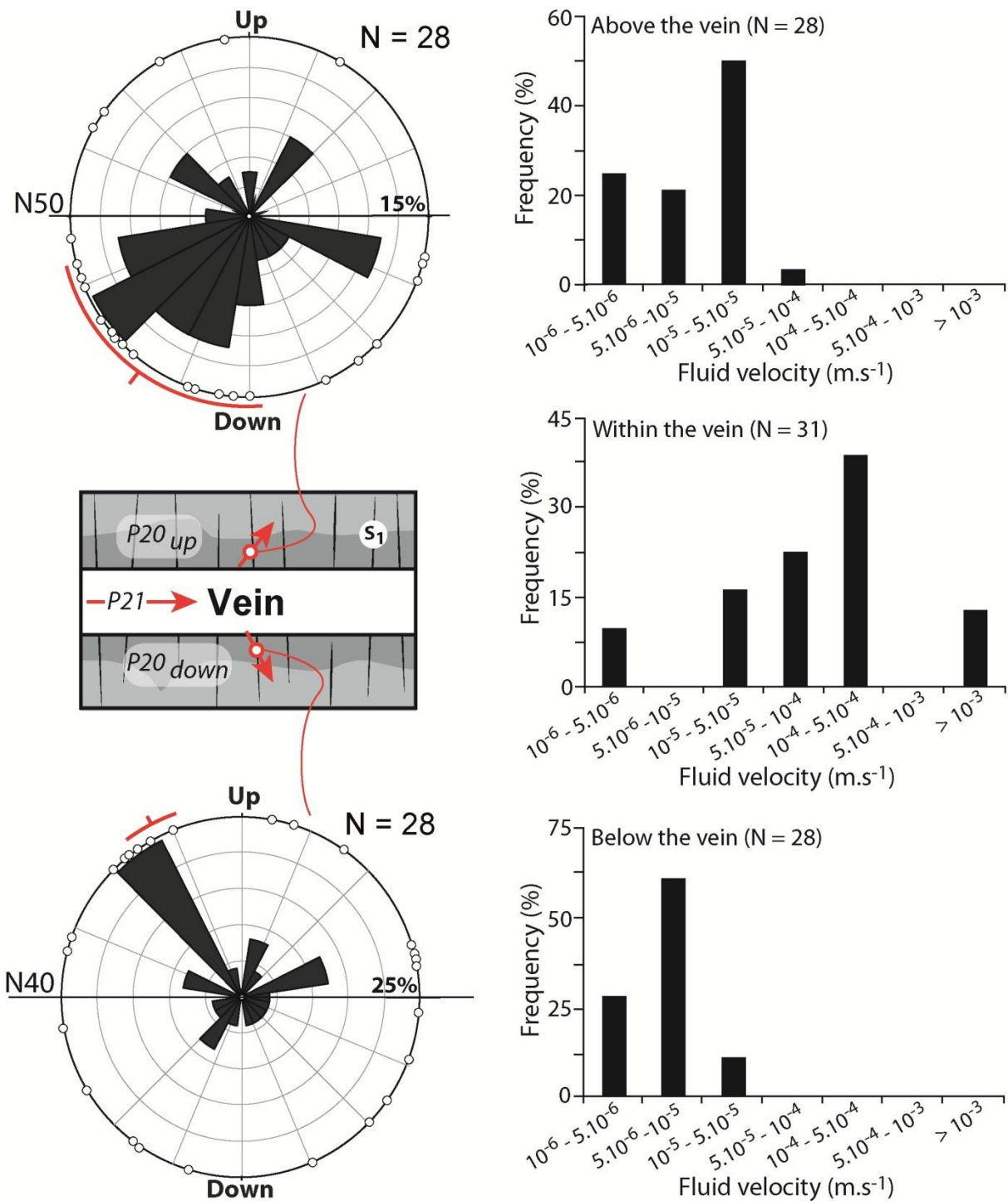


Figure 6 Sketch showing vertical paleo-fluid flow deduced from tourmaline in altered wall-rocks. Fluid flow directions are represented with rose diagrams giving direction of faces exposed to fluid flow. The red arcs indicate the 95% interval of confidence, from where the fluid comes. Velocity values obtained above, below and within the vein are presented in histogram diagrams. N corresponds to the number of measurement performed for each sample.

334

335

336

### 337 5.3 Tourmaline growth band compositions

338 Chemical compositions of tourmalines are summarized in Table 2 (complete analyses in  
339 electronic supplementary materials ESM3 and ESM4). General features and classification of  
340 Panasqueira tourmalines have already been described by Codeço *et al.*, (2017). Here, we focus on  
341 compositional differences in minor and trace elements between core and growth band used for  
342 fluid flow reconstruction. It appears that this growth band zoning is systematically associated with  
343 chemical variations in major, minor and trace elements (Table 2). In the veins, cores and rims of  
344 tourmaline exhibit compositions that suggest equilibration with Li-depleted granitic rocks (Fig.  
345 7a). However, rims are richer in Fe and poorer in Mg and Al than cores. In altered wall-rocks,  
346 cores are characterized by a wide range of compositions suggesting equilibration with  
347 metasedimentary host rocks and Li-depleted granitic rocks; whereas rims exhibit a more restricted  
348 composition identical to rims of veins-tourmalines and that suggest equilibration with Li-depleted  
349 granitic rocks (Fig. 7a). This range of core compositions (in altered wall-rocks) reflects the  
350 contribution of hydrothermal fluids and the metasedimentary host rocks during the core  
351 crystallization of tourmaline.

352 It is generally accepted that magmatic fluids contain significant amounts of Na, K and Cl. As a  
353 result, the trace element concentrations in cores and rims of tourmaline contents of core and rims  
354 of tourmaline are plotted as a function of the Na concentration to show the possible evolution of  
355 the magmatic contribution during tourmaline crystallization. Cores of tourmalines from veins and  
356 from altered wall-rocks are characterized by the same compositional ranges. This observation is  
357 also valid for rims (Table 2 and Fig. 7b). Consequently, crystallization of tourmalines in the veins  
358 is probably contemporaneous with the development of tourmalines in the altered wall-rocks. In  
359 addition, results show strong compositional differences between core and rims of tourmalines (Fig.  
360 7b). Indeed, the core to rim enrichment in Na is positively correlated with core to rim enrichments  
361 in K, Ti, Li, Mn, Sn, and Sr (Fig. 7b). Average concentrations in rims display high contents of Li,  
362 K, Mn, Ti and Zn (several hundreds to thousands of ppm) and moderate concentrations of Sn and  
363 Sr (several tens of ppm). Conversely, cores are characterized by lower trace element abundances  
364 (< 100 ppm for most elements).

365           These compositional differences between cores and rims, which are similar in the veins and in  
366 the wall-rocks, suggest that tourmalines were formed during two distinct stages. The first stage is  
367 related to core crystallization (both in veins and in wall-rocks) whereas the second stage is related  
368 to the rim overgrowths.

369           The absence of experimental partitioning coefficients between tourmaline and hydrothermal  
370 fluids do not permit to quantify the chemical signature of the hydrothermal fluid from which  
371 tourmaline has crystallized. Nevertheless, according to Van Hinsberg *et al.*, (2011a; 2017), the  
372 compositional changes between cores and growth bands provide a robust tool to track external  
373 changes in the trace-element budget of fluids from which tourmalines have crystallized. The  
374 present study suggests that rims have crystallized from a fluid richer in Na-K-Sn-Li-F-Zn than the  
375 fluid from which cores crystallized.

376

	Tourmaline from veins				Tourmaline from altered wall-rocks			
	Core		Rim		Core		Rim	
	Ave (n= 20)	Stdev	Ave (n= 20)	Stdev	Ave (n = 20)	Stdev	Ave (n = 20)	Stdev
wt%								
SiO <sub>2</sub>	35.74	0.54	35.14	0.53	34.94	1.43	35.34	0.46
TiO <sub>2</sub>	0.18	0.04	0.48	0.08	0.19	0.07	0.46	0.08
Al <sub>2</sub> O <sub>3</sub>	33.79	0.56	31.10	0.82	34.40	1.07	30.18	0.47
FeO	10.86	0.70	14.23	0.59	8.89	0.83	13.29	0.95
MnO	0.05	0.05	0.11	0.08	0.04	0.06	0.08	0.06
MgO	2.60	0.62	1.31	0.36	3.82	0.54	2.62	0.63
CaO	0.04	0.05	0.08	0.04	0.09	0.05	0.03	0.05
Na <sub>2</sub> O	1.39	0.10	2.07	0.20	1.69	0.14	2.26	0.13
K <sub>2</sub> O	0.02	0.00	0.05	0.01	0.02	0.01	0.06	0.01
F	0.00	0.01	0.00	0.00	0.00	0.00	0.00	0.00
Cl	0.00	0.00	0.01	0.01	0.01	0.01	0.01	0.01
Total	84.68		84.57		84.09		84.34	
ppm	Ave (n= 16)	Stdev	Ave (n= 17)	Stdev	Ave (n= 11)	Stdev	Ave (n= 14)	Stdev
Li	28	9.6	175	82	43	24	211	33
Na	8399	1049	17190	1739	6843	1887	14514	1463
Ti	1146	211	2465	390	2096	660	3318	269
V	84	29	98	27	61	63	55	16
Mn	413	42	698	125	171	63	542	43
Zn	545	80	908	181	302	105	853	78
Sr	14	6.3	40	9.3	29	18	41	5.5
Sn	9.6	2.9	18	6.1	9.1	6.0	14	3.8

Table 2 Summary of EPMA and LA-ICP-MS results for core and rim of tourmaline from veins and altered wall-rocks

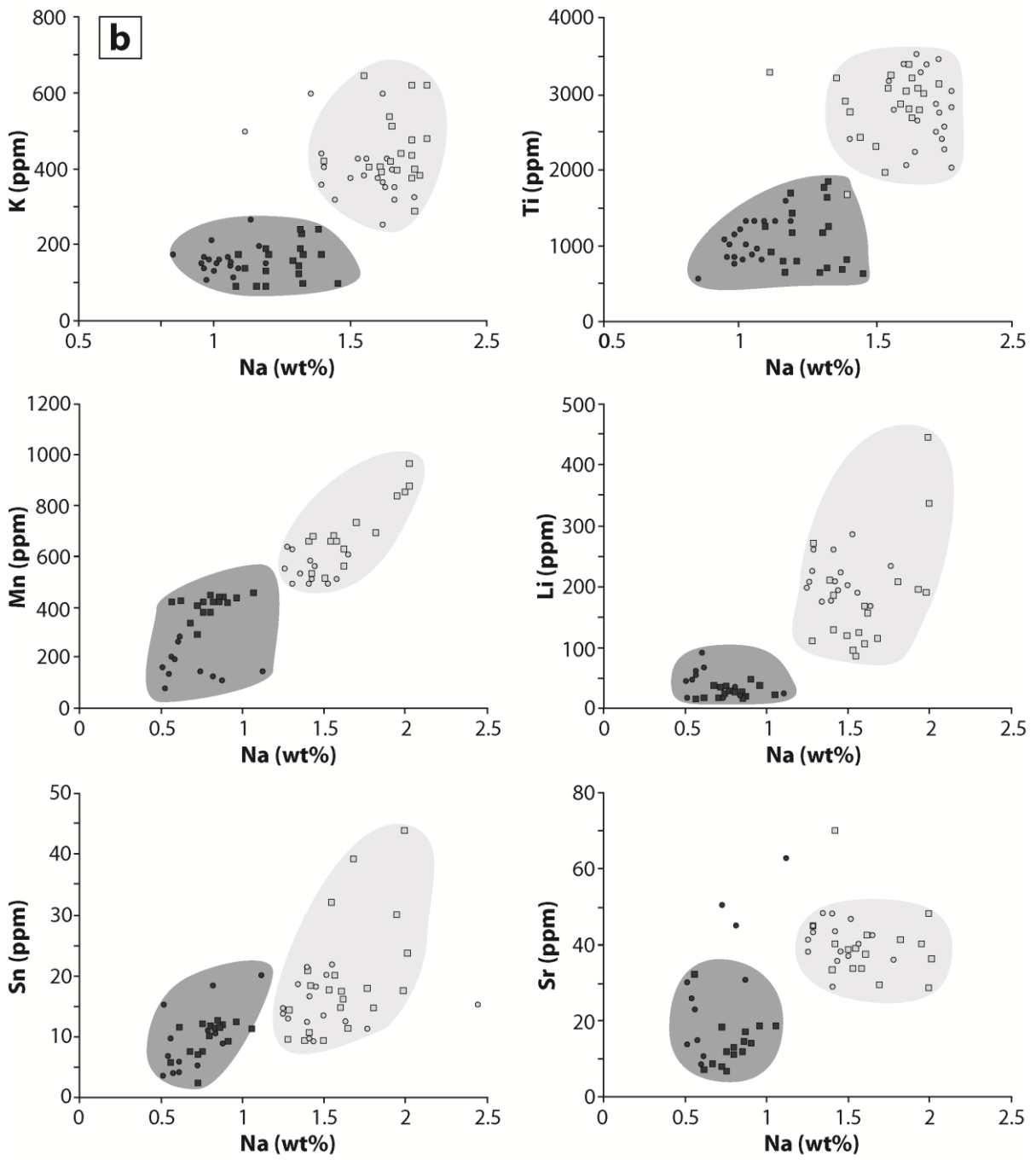
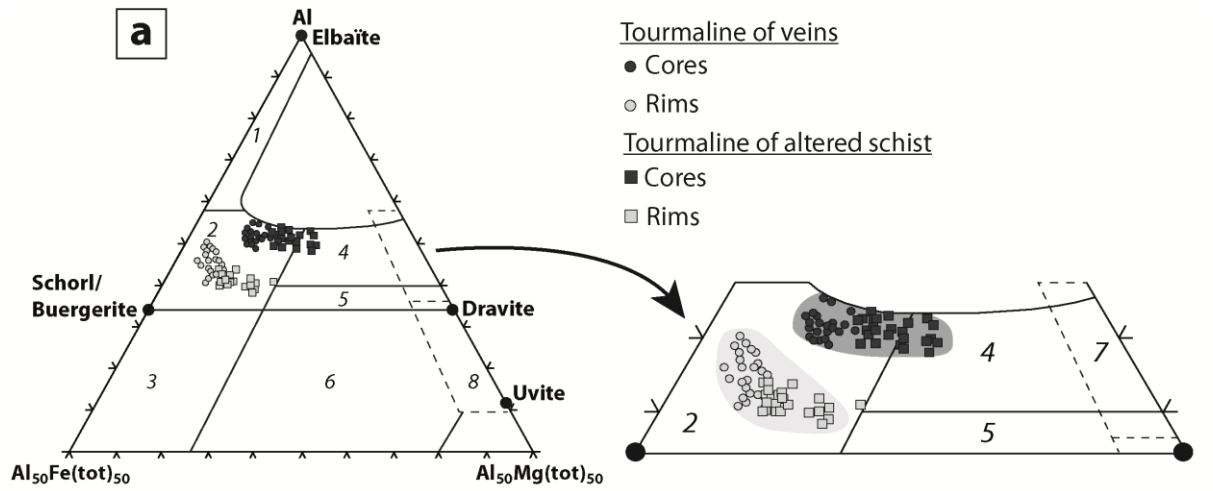


Figure 7 Geochemical characteristics of tourmalines used for fluid flow reconstruction in veins and in altered wall-rocks. (a)  $Al_{50}Fe_{50}-Al_{50}Mg_{50}$  ternary diagram showing relation between tourmaline compositions and crystallization environment (from Henry and Guidotti, 1985). (1) Li-rich granitoids, pegmatites and aplites; (2) Li-depleted granitoids, pegmatites and aplites; (3)  $Fe^{3+}$ -rich hydrothermally altered granitoids; (4) Metapelites and metapsammites with Al-saturating phase; (5) Metapelites and metapsammites without Al-saturating phase; (6)  $Fe^{3+}$ -rich metapelites and calc-silicate rocks with quartz and tourmaline; (7) Cr-V-rich metapelites and Ca-depleted meta-ultramafics rock; (8) Meta-carbonates and meta-pyroxenites. (b) Elements variation diagrams showing chemical core-rim evolution of tourmalines in minor (Na, K and Ti) and trace (Li, Mn, Sn and Sr) elements.

394

## 395 6. Discussion

### 396 6.1 Role of the granitic cupola on focusing fluid flow

397 In hydrothermal systems, fluid velocity is proportional to pressure gradient and its average  
398 direction is parallel to this gradient. Here, our spatial distribution and orientations of flow  
399 velocities suggest a high-pressure zone centered on the greisen cupola with a lateral pressure  
400 gradient triggering fluid flow in veins. Hence, hydrothermal fluids have probably been injected  
401 into the vein system from the cupola, which, consequently, represents the emanative center from  
402 where mineralizing fluids rose and spread laterally in veins. Moreover, the  $\Sigma Na/\Sigma K$  ratio  
403 determined by Poyla et al., (1989) for the ore-forming fluids (W-Sn stage) suggests an extensive  
404 interaction of these fluids with the underlying granite at 350-400 °C and 1 kbar. The rim  
405 compositions of tourmaline confirm an equilibration of fluids with granitic rocks. Furthermore, the  
406 extensive greisenisation in the apical part of the granite provides evidence of this equilibration and  
407 corroborates our interpretation of a fluid flow focused by the cupola.

408 This fluid flow pattern can explain the spatial correlation commonly observed between  
409 localization of mineralized systems and emplacement of granitic cupolas (Dines, 1956; Dilles and  
410 Proffett, 1995). Indeed, it has been proposed that magmatic fluids are preferentially expelled from  
411 cupolas, and that can disturb the pattern of convective fluid flow around intrusions by relocating  
412 convective cells and discharge zones (Norton and Cathles, 1979; Eldursi et al., 2009).  
413 Hydrothermal fluxes determined in this study provide direct evidence of the control of apices on  
414 focusing of mineralizing fluids. This behavior of fluid flow can be explained by a preferential  
415 localization of thermo-mechanical instabilities around apices (Guillou-Frottier and Burov, 2003),

416 which, when coupled with a preferential accumulation of fluids, leads to opening of permeable  
417 structures in which mineralizing fluids are then discharged.

418 Hence, the apical parts of plutonic intrusions represent convergence spots for hydrothermal  
419 fluids and thus are favorable zones for deposition of high grade mineralization. As a result, the  
420 approach applied in this study can be useful for mining exploration as pathfinder to discover  
421 hidden granitic cupolas and thus locate the emanative centers of mineralizing fluids.

## 422 *6.2 Fluid escape in wall-rocks and role of fluid on vein opening*

423 The vertical escape of fluids from veins toward metasedimentary host rock involves a vertical  
424 pressure gradient with overpressured fluid conditions in veins, causing pervasive fluid flow in the  
425 wall-rocks. This interpretation is consistent with the presence of alteration fronts observed around  
426 veins (Fig. 3a). Besides, Lecumberri-Sanchez et al., (2017) have demonstrated that schists  
427 proximal to the veins are systematically enriched in K, B, Sn and W. The rims of tourmalines  
428 present in altered wall-rocks are also enriched in certain of these elements (K and Sn). This is  
429 consistent with extensive fluid–rock interaction triggered by fluids coming from veins.

430 According to the rim compositions of vein-and schist-tourmalines, fluid flow in veins can be  
431 considered contemporaneous with pervasive fluid flow in altered wall-rocks. As shown above,  
432 fluid flow in wall-rocks is related to overpressured conditions in veins. Thus, our results suggest  
433 that veins opening and dilation have been induced by injection of fluids at supralithostatic  
434 conditions such as proposed by Foxford et al., (2000). The low velocity values (not exceeding  
435  $5.10^{-5} \text{ m.s}^{-1}$ ) obtained in altered wall-rocks imply a low permeability in the host rocks. As a result,  
436 the element transport through the host rock was probably low and limited to the alteration haloes.

437 Based on the removal of iron (Fe) from the wall-rocks during fluid-rock interactions,  
438 Lecumberri-Sanchez et al., (2017) suggest that some elements such as Fe have migrated from the  
439 host rocks toward veins. At first sight, this chemical flux seems to be incompatible with the  
440 direction of fluid flow discussed above. However, iron migration through the host rocks was  
441 probably driven by diffusion following a strong chemical gradient between fluid in veins and  
442 metasedimentary host rocks, whereas fluid flow was driven by pressure gradient. These two

443 processes have not involved the same driving force, and it is, therefore, possible to observe a  
444 chemical flux that is characterized by a vector that is opposed to the fluid flow direction.

### 445 *6.3 Velocity analysis and estimation of fluid flow duration during the QTS-MOSS*

446 In this study, the mean fluid flow velocity deduced from veins tourmalines ( $10^{-4}$  m.s<sup>-1</sup>) is high  
447 and close to values obtained with the same method in the same type of deposit by Sizaret *et al.*,  
448 (2009) and Mahjoubi *et al.*, (2016), and suggests an efficient metal transport in veins. Considering  
449 a porous media with an averaged porosity of 1%, the conversion of this mean velocity to a Darcy  
450 velocity ( $V_{\text{Darcy}} = V \cdot \text{porosity}$ ) gives a value of  $10^{-6}$  m.s<sup>-1</sup>. Darcy velocities obtained in contact  
451 metamorphic aureoles from mineral reactions and by numerical modeling range respectively from  
452  $10^{-9}$  to  $10^{-11}$  m.s<sup>-1</sup> (Ferry *et al.*, 2002), and from  $10^{-8}$  to  $10^{-11}$  m.s<sup>-1</sup> (Eldursi *et al.*, 2009). It appears  
453 that velocities obtained in this study are 2 to 5 order of magnitude higher than those deduced from  
454 mineral reactions and numerical modeling. This difference may be due to the fact that velocities  
455 obtained from mineral growth bands are valid for a specific hydrothermal stage occurring over a  
456 short period of time, while those deduced from other methods are integrated over a larger scale  
457 and for the total duration of the hydrothermal system (Ingebritsen and Manning, 1999).

458 It is widely agreed that the overall time span of hydrothermal activity encompasses multiple  
459 fluid pulses, each of them occurring over only a short period of time. If geochronological methods  
460 allow dating hydrothermal activity, the uncertainties of these analytical methods do not always  
461 permit the estimation of the fluid flow duration for a specific stage. As in most cases, the  
462 Panasqueira deposit was formed during a long period of time lasting about 4.2 Myr (Snee *et al.*,  
463 1988) but subdivided into several pulses. Here we propose the use of the mean fluid velocity value  
464 obtained from veins-tourmaline to estimate the fluid flow duration required for the vein formation  
465 during the QTS and MOSS. To do this, we assume that the QTS and the MOSS were formed  
466 during the same continuous hydrothermal event with a constant fluid flow velocity. According to  
467 Poyla *et al.*, (1989) the total volume of fluid that flowed through the vein system during the MOSS  
468 is about 1000 km<sup>3</sup> with 0.2 ppm of dissolved WO<sub>3</sub>. Considering a total volume of vein about 0.003  
469 to 0.006 km<sup>3</sup> extending over an area of 6 km<sup>2</sup> (Hebblethwaite and Antao, 1982) characterized by  
470 an elliptical shape, we can calculate the surface of the vertical section of fluid flow. From this

471 surface and the mean fluid flow velocity ( $10^{-4} \text{ m.s}^{-1}$ ) we obtain a fluid flow duration ranging from  
472 35 000 to 70 000 years. This is consistent with the short time duration of mineralization  
473 emplacement estimated for a single magmatic-hydrothermal event (spanning only about 10 000 to  
474 200 000 years) from numerical modeling (Cathles *et al.*, 1997; Chelle-Michou *et al.*, 2017) and  
475 radiometric dating (Parnell, 1998).

#### 476 *6.4 Hydrodynamic model of the Panasqueira deposit*

477 Our results must be considered as ‘snapshot’ of the fluid flow at the incipient phase of the  
478 hydrothermal system of Panasqueira, corresponding to the magmatic-hydrothermal transition.  
479 Considering chemical characteristics of tourmalines and our fluid flow reconstruction, a  
480 hydrodynamic model subdivided into two stages is proposed for the early hydrothermal event  
481 preceding the main stage of W-Sn mineralization (Fig. 8). The first stage is related to the core  
482 crystallization of tourmalines and involves an initial flow of boron-rich fluids. These fluids are  
483 partly buffered by the metasedimentary host rocks for Al, Mg and Fe during the crystallization of  
484 tourmaline in the wall-rocks (Fig. 7a). This first pulse does not seem to be associated with any  
485 W-Sn mineralization. This is consistent with the low contents in trace elements in cores of  
486 tourmaline. We have no information about directions of fluid flow related to this first pulse.  
487 However, the chemical equilibration of cores of veins-tourmalines with Li-depleted granitic rocks  
488 suggests that the first stage can be related to a first expulsion of magmatic fluid during granite  
489 crystallization.

490 The second stage is recorded by tourmaline growth bands and is related to the flow of the  
491 mineralized (Li-K-Na-Sn)-rich fluid in the veins system. During this second stage, the external  
492 convecting fluids and magmatic fluids released by granite crystallization are both focused by the  
493 cupola, which causes the greisenization in the apical part of the granite (Fig. 8). This focused fluid  
494 flow is injected into the vein system, whose the significant horizontal permeability anisotropy  
495 induces a horizontal fluid flow along the vein planes. The low permeability of the  
496 metasedimentary host rock promotes fluid pressure increase leading to the vein opening when  
497 fluid pressure reaches supralithostatic conditions (Fig. 8). The velocity contrast between veins ( $10^{-4}$   
498 to  $10^{-3} \text{ m.s}^{-1}$ ) and altered wall-rocks ( $10^{-6}$  to  $10^{-5} \text{ m.s}^{-1}$ ) emphasize this strong contrast of

499 permeability and suggests that fluid flow was mainly channeled in the vein system. This  
 500 channelization of mineralizing fluids in veins could contribute to form a high grade deposit by an  
 501 efficient metal transport in structural trap sites. The overpressured condition in veins enhances  
 502 fluid-rock interaction and triggers a pervasive fluid migration in the wall-rocks (Fig. 8). According  
 503 to Lecumberri-Sanchez *et al.*, (2017), the metasedimentary host rock is mainly affected by  
 504 tourmalinization and muscovitization reactions, which are crucial for the wolframite deposition by  
 505 iron releasing into the fluid. Finally, the escape of fluids toward the wall-rocks observed in this  
 506 study can constitute a crucial mechanism for the wolframite deposition by promoting fluid-rock  
 507 interactions.

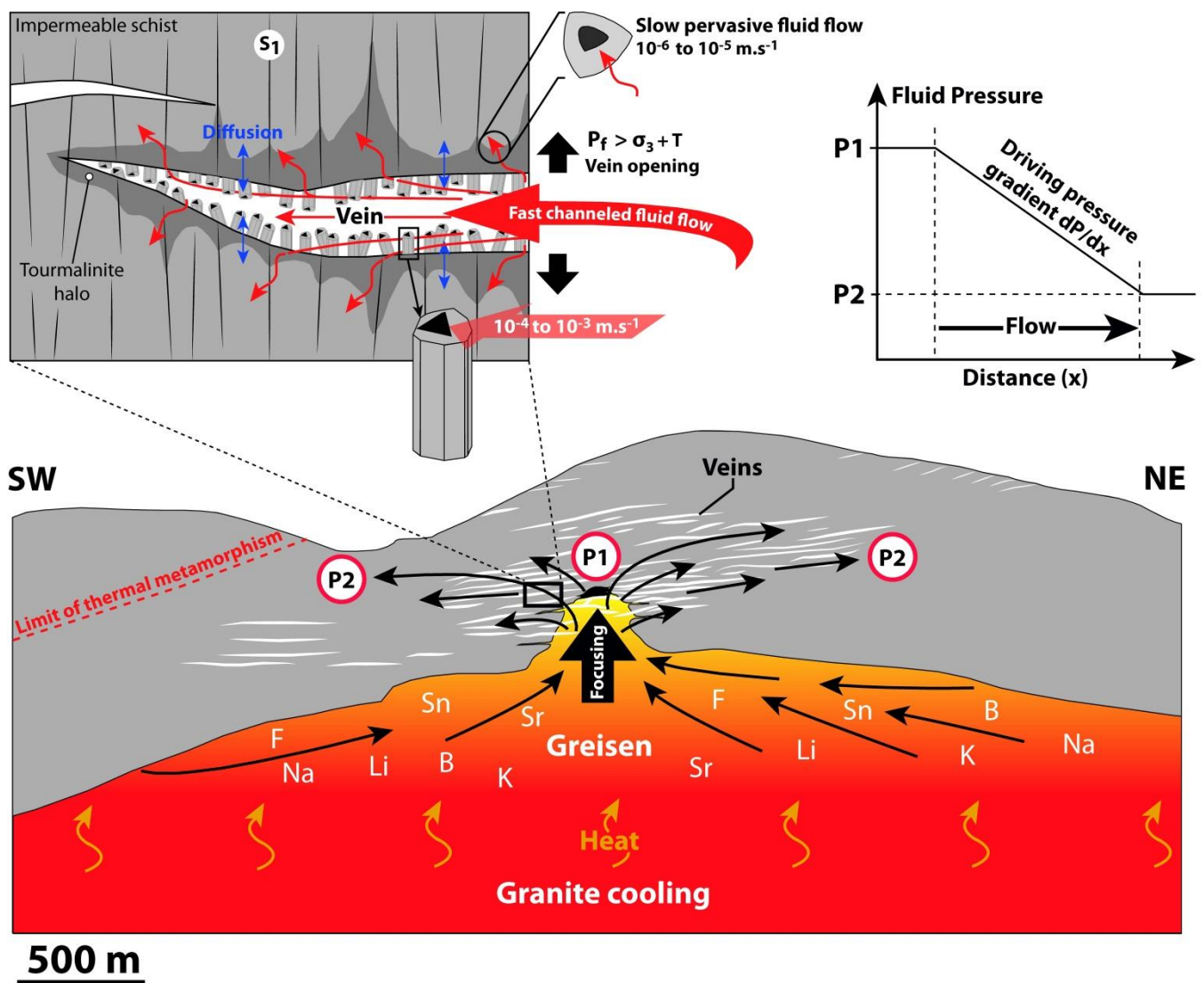


Figure 8 Hydrodynamic model of fluid flow at the magmatic-hydrothermal transition of the W-Sn-(Cu) Panasqueira deposit (drafted on simplified cross section from Thadeu, 1951). With  $P_f$ : the fluid pressure condition,  $\sigma_3$ : the vertical stress and  $T$ : the tensile strength.

508           **Acknowledgments**

509           We are greatly thankful to Beralt Tin & Wolfram S.A. for the possibility to access to the  
510 Panasqueira underground mine. We thank Paolo Ferraz for help during the collection of samples  
511 in mine and for discussions about our results. We further would like to thank P. Lach for  
512 assistance in LA-ICP-MS analyses and proceeding of data. We are grateful to anonymous  
513 reviewers for their constructive remarks, which have greatly improved this manuscript. This  
514 research was financially supported by the French Geological Survey (BRGM), Region Centre, the  
515 Labex Voltaire (ANR-10-LABX-100-01) and has also taken part of the ERAMIN project “New  
516 Ores”.

517           **References**

- 518 Barnes, H.L. 1997. *Geochemistry of Hydrothermal Ore Deposits*, third ed. John Willey and Sons,  
519 New York.
- 520 Bishop, A.C. 1989. Greisen. In: *Petrology. Encyclopedia of Earth Science*. Springer, Boston, MA.
- 521 Bussink, R.W. 1984. *Geochemistry of the Panasqueira Tungsten-Tin Deposit, Portugal*. Geol.  
522 Ultraiectina.
- 523 Cartwright, I., Buick, I.S. 1996. Determining the direction of contact metamorphic fluid flow: an  
524 assessment of mineralogical and stable isotope criteria. *J. Metamorph.Geol.* 14, 289–305.
- 525 Cathles, L.M., Erendi, A.H.J. & Barrie, T. 1997. How long can a hydrothermal system be  
526 sustained by a single intrusive event? *Econ. Geol.*, 92: 766-771.
- 527 Černý, P., Blevin, P.L., Cuney, M. and London, D. 2005. Granite-Related Ore Deposits. In: J.W.  
528 Hedenquist, J.F.H. Thompson, R.J. Goldfarb, and J.R. Richards (eds.). *Economic Geology -*  
529 *One Hundredth Anniversary Volume*, 337–370.
- 530 Chelle-Michou, C., Rottier, B., Caricchi, L. and Simpson, G. 2017. Tempo of magma degassing  
531 and the genesis of porphyry copper deposits. *Nature Scientific Reports* 7,  
532 Article number: 40566.
- 533 Clark, A. H. 1964. Preliminary study of the temperatures and confining pressures of granite  
534 emplacement and mineralization, Panasqueira, Portugal: *Inst. Mining MetallurgyTrans.*, 73,  
535 813-824.

- 536 Codeço, M., Weis, P., Trumbull, R., Pinto, F., Lecumberri-Sanchez, P., Wilke, F. 2017. Chemical  
537 and boron isotopic composition of hydrothermal tourmaline from the Panasqueira W-Sn-Cu  
538 deposit, Portugal. - *Chemical Geology* (online).
- 539 Cox, S.J. 2005. Coupling between Deformation, Fluid Pressures, and Fluid Flow in Ore-  
540 Producing Hydrothermal Systems at Depth in the Crust. In: J.W. Hedenquist, J.F.H.  
541 Thompson, R.J. Goldfarb, and J.R. Richards (eds.). *Economic Geology - One Hundredth*  
542 *Anniversary Volume*, 39–75.
- 543 Curie P. 1908. *Œuvres*, 118p. Gautier-Villars, Paris, Société Française de Physique. Reprinted:  
544 *Archives contemporaines*, Paris 1984.
- 545 Derré, C. 1982. Caractéristiques de la distribution des gisements à étain-tungstène dans l'ouest de  
546 l'Europe. *Mineral. Deposita* 17:55-77.
- 547 Dias, R. & Ribeiro, A. 1995. The Ibero Armorican Arc: a collision effect against an irregular  
548 continent? *Tectonophysics*, 246: 113-128
- 549 Dias, G., Leterrier, J., Mendes, A., Simões, P., Bertrand, J.M. 1998. U-Pb zircon and monazite  
550 geochronology of syn- to post-tectonic Hercynian granitoids from the central Iberian Zone  
551 (northern Portugal). *Lithos* 45, 349–369.
- 552 Dilles, J.H., Profett, J.M. 1995. Metallogensis of the Yerington batholith, Nevada, in: F.W.  
553 Pierce, J.G. Bolm (Eds.), *Porphyry Copper Deposits of the American Cordillera*, American  
554 Geological Society Digest 20, , pp. 306-315.
- 555 Dines, H.G. 1956. *The metalliferous mining region of South-West England*. 2 volumes, HMSO,  
556 London.
- 557 Eldursi, K., Branquet, Y., Guillou-Frottier, L., Marcoux, E. 2009. Numerical investigation of  
558 transient hydrothermal processes around intrusions: Heat-transfer and fluid-circulation  
559 controlled mineralization patterns. *Earth and Planetary Science Letters* 288, 70-83.
- 560 Ferry, J., Wing, B., Penniston-Dorland, S., Rumble, D. 2002. The direction of fluid flow during  
561 contact metamorphism of siliceous carbonate rocks: new data for the Monzoni and Predazzo  
562 aureoles, northern Italy, and a global review. *Contrib. Mineral. Petr.* 142,679-699.
- 563 Foxford, K.A., Nicholson, R., Polya, D.A., Hebblethwaite, R.P.B. 2000. Extensional failure and  
564 hydraulic valving at Minas da Panasqueira, Portugal: Evidence from vein spatial  
565 distributions, displacements and geometries. *J. Struct. Geol.* 22, 1065-1086.
- 566 Gloaguen, E., Branquet, Y., Chauvet, A., Bouchot, V., Barbanson, L. and Vignerresse, J.L. 2014.  
567 *Tracing the Magmatic/Hydrothermal Transition in Regional Low-Strain Zones: The Role of*

- 568 Magma Dynamics in Strain Localization at Pluton Roof, Implications for Intrusion-Related  
569 Gold Deposits. *Journal of Structural Geology* 58: 108–121.
- 570 Guillou-Frottier, L., Burov, E. 2003. The development and fracturing of plutonic apices:  
571 implications for porphyry ore deposits. *Earth & Planetary Science Letters*, 214, 341-356.
- 572 Hebblethwaite, R. P. B., and Antao, A.M. 1982. A report on the study of dilation patterns within  
573 the Panasqueira ore body: Barroca Grande, Beralt Tin Wolfram (Portugal), unpub. rept.15p.
- 574 Hedenquist, J.W., Lowenstern, J.B. 1994. The role of magma in the formation of hydrothermal  
575 ore deposits. *Nature* Vol. 370: 519-526.
- 576 Henry, D.J., Guidotti, C.V. 1985. Tourmaline as a petrogenetic indicator mineral: an example  
577 from the staurolite-grade metapelites of NW Maine. *Am. Mineral.* 70,1–15.
- 578 Henry, D.H., Dutrow B. L. 1996. Metamorphic tourmaline and its petrologic applications.  
579 *Reviews in Mineralogy and Geochemistry* 33 (1): 503-557.
- 580 Ingebritsen, S.E., Manning, C.E. 1999. Geologic implications of a permeability–depth curve for  
581 continental crust. *Geology* 27, 1107–1110.
- 582 Ingebritsen, S.E., Appold, M.S. 2012. The physical hydrogeology for ore deposits. *Econ Geol*  
583 107:559–584
- 584 Julivert, M., Fontboté, J.M., Ribeiro, A., Conde, L. 1972. Mapa Tectonico de la Peninsula Iberica  
585 y Baleares E. 1:1.000.000. *Inst. Geol. Min. España, Madrid.*
- 586 Kelly, W.C., Rye, R.O. 1979. Geologic, fluid inclusion and stable isotope studies of the tin-  
587 tungsten deposits of Panasqueira, Portugal. *Econ Geol* 74:1721–1822
- 588 Kessler, S.E., Stoiber, R.E. & Billings, G.K. 1972. Direction of flow mineralizing solutions at  
589 Pine Point, N.W. T., *Econ. Geol.*, **67**, 19–24.
- 590 Lecumberri-Sanchez, P., Vieira, R., Heinrich, C.A., Pinto, F., Wälle, M. 2017. Fluid-rock  
591 interaction is decisive for the formation of tungsten deposits. *Geology* 45, 579-582.
- 592 Mahjoubi, E.M., Chauvet, A., Badra, L., Sizaret, S., Barbanson, L., El Maz1, A., Chen, Y., and  
593 Amann, M. 2016. Structural, mineralogical, and paleoflow velocity constraints on Hercynian  
594 tin mineralization: the Achmmach prospect of the Moroccan Central Massif. *Miner. Deposita*  
595 51: 431.
- 596 Marks, M. A. W., Schühle, P., Guth, A., Wenzel, T. and Markl, G. 2013. Trace element  
597 systematics of tourmaline in pegmatitic and hydrothermal systems from the Variscan  
598 Schwarzwald (Germany) : the importance of major element composition, sector zoning, and  
599 fluid or melt composition. *Chemical geology*, Vol. 344, p.73-90.

- 600 Martinez Catalan, J.R., Arenas, R., Diaz Garcia, F., et al. 2007. Space and time in the tectonic  
601 evolution of the northwestern Iberian Massif: Implications for the Variscan belt. In: Hatcher  
602 RD, Carlson MP, McBride JH, Martínez Catalán JR (eds) 4-D Framework of continental  
603 crust: Geological Society of America Memoir 200. Geological Society of America, 403–423
- 604 Norton, D., Cathles, L.M. 1979. Thermal aspects of ore deposition. In: Barnes, H.L. (Ed.),  
605 Geochemistry of Hydrothermal Ore Deposits, second ed. John Wiley and Sons, New York,  
606 pp. 611–631.
- 607 Parnell, J. 1998. Dating and Duration of Fluid Flow and Fluid–Rock Interaction.: Geological  
608 Society Special Publication, 144, 284 pp
- 609 Polya, D.A. 1989. Chemistry of the main-stage ore-forming fluids of the Panasqueira WCu(Ag)-  
610 Sn deposit, Portugal: implications for models of ore genesis. *Econ. Geol.* 84, 1134–1152.
- 611 Polya, D.A., Foxford, K.A., Stuart, F., Boyce, A., Fallick, A.E. 2000. Evolution and paragenetic  
612 context of low  $\delta D$  hydrothermal fluids from the Panasqueira W-Sn deposit, Portugal: New  
613 evidence from microthermometric, stable isotope, noble gas and halogen analyses of primary  
614 fluid inclusions. *Geochim. Cosmochim. Acta* 64, 3357–3371.
- 615 Robb, L. 2005. Introduction to Ore-forming Processes. Blackwell Publishing, Malden, MA, 373  
616 p.
- 617 Sams, M. S. & Thomas-Betts, A. 1988. Models of convective fluid flow and mineralization in  
618 Southwest England. *Journal of the Geological Society.* 145, 809–817.
- 619 Shcherba, G. N. 1970. Greisens. *Int Geol Rev* 12: 114–255
- 620 Sibson, R.H. 1992. Implications of fault-valve behaviour for rupture nucleation and recurrence.  
621 *Tectonophysics*, 211, 283–93.
- 622 Sizaret, S., Fedioun, I., Barbanson, L., Chen, Y. 2006. Crystallization in flow part II: modelling  
623 crystal growth kinetics controlled by boundary layer thickness. *Geophys J Int* 167:1027–  
624 1034
- 625 Sizaret, S., Branquet, Y., Gloaguen, E., Chauvet, A., Barbanson, L., Chen, Y. 2009. Estimating  
626 the local paleo-fluid flow velocity: new textural method and application to metasomatism.  
627 *Earth Planet Sci Lett* 280:71–82.
- 628 Snee, L.W., Sutter, J.F., Kelly, W.C. 1988. Thermochronology of economic mineral deposits;  
629 dating the stages of mineralization at Panasqueira, Portugal, by high-precision  $^{40}\text{Ar}/^{39}\text{Ar}$   
630 age spectrum techniques on muscovite. *Econ Geol* 83:335–354
- 631 Thadeu, D. 1951. Geologia do couro mineiro da Panasqueira. *Comunic Serv Geol Port* 32:5–64.

- 632 Van Hinsberg, V.J., Henry, D.J., Dutrow, B.L. 2011a. Tourmaline as a Petrologic Forensic  
633 Mineral: A Unique Recorder of Its Geologic Past. *Elements* 7, 327–332.
- 634 Van Hinsberg, V.J., Franz, G. and Wood, B.J. 2017. Determining subduction-zone fluid  
635 composition using a tourmaline mineral probe. *Geochemical Perspectives Letters* v3, n1.
- 636 Weis, P. 2015. The dynamic interplay between saline fluid flow and rock permeability in  
637 magmatic-hydrothermal systems. *Geofluids*, 15, 350-371.
- 638 Whitney, D.L, Evans, B.W. 2010. Abbreviations for names of rock-forming minerals. *Am.*  
639 *Mineral* 95:185-187.